ChemComm

COMMUNICATION

View Article Online
View Journal

Check for updates

Cite this: DOI: 10.1039/c7cc04052k

Received 25th May 2017,
Accepted 6th July 2017

DOI: 10.1039/c7cc04052k

rsc.li/chemcomm

Published on 06 July 2017. Downloaded by Cornell University Library on 18/07/2017 13:28:58.

Development and photocatalytic mechanism of monolayer Bi_2MoO_6 nanosheets for the selective oxidation of benzylic alcohols†

Kaiqiang Jing,[a] Jinhua Xiong,[a] Na Qin,[a] Yujie Song,[a] Liuyi Li,[b] Yan Yu,[b] Shijing Liang *[a] and Ling Wu *[ab]

Monolayer Bi_2MoO_6 nanosheets have been successfully prepared for the first time *via* a bottom-top approach with surfactant assistance, and show 8 times higher activity than bulk Bi_2MoO_6 for the selective oxidation of benzyl alcohol. Ultrafast charge separation and more acid–base active sites on the monolayer nanosheets are considered to be responsible for the robust photoactivity.

Heterogeneous photocatalysis is regarded as a significant process in clean energy production, environmental modification and fine chemical synthesis.[1–4] Very recently, monolayer nanosheets have drawn immense attention owing to their distinctive characteristics, such as larger surface areas, more active sites, molecular thickness and ultrafast charge separation, that give them improved performance in heterogeneous photocatalysis compared to their bulk materials.[5–7] Benefiting from the structure of two dimensional (2D) nanosheets with monolayer thickness, they possess an increased charge density of states on the outmost layer of the monolayer nanosheets, in contrast to their bulk materials.[8] Therefore, active electrons and acid–base active sites that are primarily from the surface of the monolayer could preferably participate in the photocatalytic reaction and provide the prerequisite for interactions with the reactants.[8,9] Recently, Aurivillius phase bismuth-based nanosheets have attracted considerable attention due to their non-toxicity, suitable band gaps and high quantum yield for photocatalysis under visible-light irradiation.[10–12] Among these materials, orthorhombic Bi_2MoO_6, a unique layered structure that is constructed by alternating $(Bi_2O_2)^{2+}$ and $(MoO_4)^{2-}$ perovskite layers, has emerged as a promising candidate.[13] More importantly, orthorhombic Bi_2MoO_6 has suitable valence band and conduction band potentials. These make it feasible to transform organics, especially alcohols, into their corresponding aldehydes.[14] However, bulk Bi_2MoO_6 usually has poor photocatalytic efficiency and selectivity, which is primarily attributed to the rapid recombination of photogenerated charges and the fact that there are relatively few surface active sites.[15] From the above properties, single molecular Bi_2MoO_6 may shed light on resolving these problems, since abundant active sites and effective charge separation play crucial roles in the process of delivering electrons from the inside layer to the surface. Moreover, it is indispensable to understand photocatalytic reactions at the molecular level for monolayer materials.[16,17]

Herein, we report a cetyltrimethylammonium bromide (CTAB)-assisted bottom-up method to firstly synthesize the monolayer Bi_2MoO_6 nanosheets. The detailed preparation procedure is described in the ESI† (Experimental section). The X-ray diffraction patterns of the resulting samples are shown in Fig. S1 (ESI†). All of the diffraction peaks can be indexed to an orthorhombic Bi_2MoO_6 phase with lattice parameters a = 5.502 Å, b = 16.213 Å and c = 5.483 Å (JCPDS No. 21-0102). Moreover, the XRD patterns of the prepared samples are similar to those of the bulk materials, but they have much weaker and broader intensities than those of the bulk materials. Notably, the intensity of the diffraction peak at 2θ = 10.92° (corresponding to the characteristic peak (020)) of the prepared sample is much lower than that of the bulk counterpart. This implies that the thickness of the prepared sample is greatly decreased in the b-axis direction compared to that of the bulk counterpart, and the sample loses its periodic layered structure. The SEM images (Fig. S2a and b, ESI†) clearly show that Bi_2MoO_6 contains a typical layer structure. The TEM image in Fig. 1a shows that it possesses a sheet-shaped structure with a lateral size of 300 nm. The HRTEM image (the inset in Fig. 1a) reveals the marked interplanar spacings of the (200) and (002) planes, which further indicate the bottom-top facets of the Bi_2MoO_6 sample. As shown in Fig. 1b, the SAED pattern reveals that it possesses single crystalline features. A series of bright spots can be indexed to the [020] zone axis of the prepared sample. The atomic force microscopy (AFM) images and the corresponding height profiles show that the sample has an average thickness of 0.82 nm (Fig. 1c and d), which agrees well with the 0.84 nm thickness of a single-layered

[a] State Key Laboratory of Photocatalysis on Energy and Environment, Fuzhou University, Fuzhou 350116, P. R. China. E-mail: sjliang2011@gmail.com, wuling@fzu.edu.cn; Tel: +86-591-22865835

[b] Key Laboratory of Eco-materials Advanced Technology (Fuzhou University), Fujian Province University, Fuzhou University, Fuzhou 350116, P. R. China

† Electronic supplementary information (ESI) available. See DOI: 10.1039/c7cc04052k

Published on 06 July 2017. Downloaded by Cornell University Library on 18/07/2017 13:28:58.

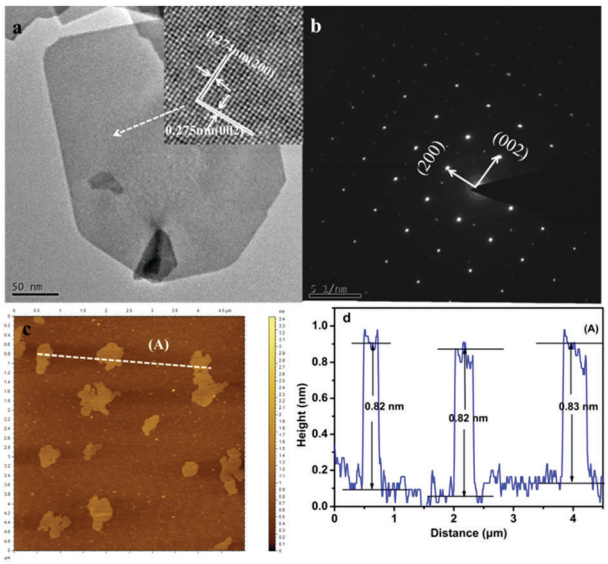

Fig. 1 Characterization of the monolayer Bi_2MoO_6 nanosheet. (a) A TEM image, where the inset is the corresponding HRTEM image, (b) the SAED pattern, (c) an AFM image and (d) the corresponding thickness analysis that was taken around the white line in (c).

Bi_2MoO_6 nanosheet along the [020] direction (Fig. S3, ESI†), providing direct and solid evidence for the formation of monolayer Bi_2MoO_6 nanosheets. Furthermore, both the TEM image (Fig. S4a, ESI†) and the HRTEM image (Fig. S4b, ESI†) show that bulk Bi_2MoO_6 has a rectangular plate structure. This indicates that CTAB is beneficial for forming the monolayer nanosheets, and that the concentration of Br^- ions plays an important part in preventing the monolayers from stacking.[18] Furthermore, although Bi_2MoO_6 nanosheets were also prepared in a previous report *via* solvothermal reactions using SDS, PVP and CTAB as surfactants and ethylene glycol as a solvent,[19] the thicknesses of the reported Bi_2MoO_6 nanosheets were much higher than the thickness of our sample.

XPS was conducted to confirm the chemical composition of the monolayer Bi_2MoO_6 nanosheets. The Bi 4f, Mo 3d, O 1s and Br 3d XPS spectra of the Bi_2MoO_6 monolayer and bulk are shown in Fig. S5 (ESI†). The Bi 4f spectra (Fig. S5a, ESI†) exhibit two contributions, $4f_{7/2}$ and $4f_{5/2}$ (resulting from spin–orbit splitting), located at 159.2 and 164.4 eV, respectively,[20,21] which can be assigned to Bi^{3+}. Fig. S5b (ESI†) shows that the binding energies for the Mo $3d_{5/2}$ and Mo $3d_{3/2}$ of Mo^{6+} are around 232.5 and 235.6 eV, respectively.[22] These results indicate that the chemical states of Bi^{3+} and Mo^{6+} are almost comparable for the two samples. Fig. S5c (ESI†) shows O 1s spectra, and the peaks located at 530.1 and 531.4 eV can be ascribed to lattice oxygen and bridging hydroxyls, respectively.[23] However, in contrast to bulk Bi_2MoO_6, the binding energy of O 1s attributed to lattice oxygen over the monolayer Bi_2MoO_6 nanosheets reduces by 0.11 eV, which may result from the decrease of the Bi–O and Mo–O bond orders when Br^- ions interact with $[Bi_2O_2]^{2+}$, thus improving the charge density on the outer-most layer over the monolayer Bi_2MoO_6 nanosheets.[24] At the same time, the XPS peak of O 1s that belongs to the adsorbed hydroxyl species over the monolayers reduces by 0.3 eV. This may be due to the fact that the Br^- ions intimately interact with the Bi_2MoO_6 layer and the feature of the monolayer nanosheets. It is worth noting that the amount of adsorbed hydroxyl species is smaller than that of the bulk counterpart. This may be because the Br^- ions adsorbed on the surface of Bi_2MoO_6 decrease the amount of adsorption sites for the hydroxyl species. The Br/Bi/Mo ratio on the monolayer Bi_2MoO_6 nanosheets is 0.2/2.3/1.0, confirmed by quantitative XPS analysis, which is nearly identical to the bulk with respect to the Bi/Mo ratio. This result indicates that the Br^- ions may interact with $[Bi_2O_2]^{2+}$ in a non-stoichiometrical manner.

Using the Bi_2MoO_6 monolayers and bulk Bi_2MoO_6 as heterogeneous photocatalysts, their performance for the selective oxidation of benzyl alcohol (BA) was evaluated under visible light irradiation ($\lambda \geq 400$ nm). The monolayers have much higher visible-light-driven photocatalytic activity than the bulk. 26.5% of benzyl alcohol was converted to benzaldehyde using the monolayers as the photocatalyst within 4 h (Fig. 2a), while only 3.2% of benzyl alcohol was converted to benzaldehyde using the bulk Bi_2MoO_6 as the photocatalyst within 4 h (Table S1, ESI†, entry 1). Moreover, only benzaldehyde could be detected for the oxidation of BA on the Bi_2MoO_6 samples. These monolayer Bi_2MoO_6 nanosheets also exhibit superior photocatalytic activity in contrast to most of the reported Bi_2MoO_6 samples (Table S2, ESI,† entries 8 and 9). More intriguingly, it was found that the monolayers had much higher photocatalytic performances than bulk Bi_2MoO_6 for *para*-substituted benzyl alcohols containing different groups such as OCH_3, CH_3, F and Cl (Fig. 2a and Table S1, ESI,† entries 2–5). In particular, it is worth noting that electron-donating groups (such as CH_3 and OCH_3) are more easily oxidized than samples containing electron-withdrawing groups (such as F and Cl). It is demonstrated that O_2, visible light and Bi_2MoO_6 are necessary for the oxidation of BA (Fig. 2a and Table S2, ESI,† entries 1–4). There was no apparent loss in the catalytic activity during three consecutive runs (Fig. S6, ESI†) and the XRD patterns (Fig. S7, ESI†) of the fresh and used samples are almost the same, both of which indicate that the monolayer nanosheets possess stable durability.

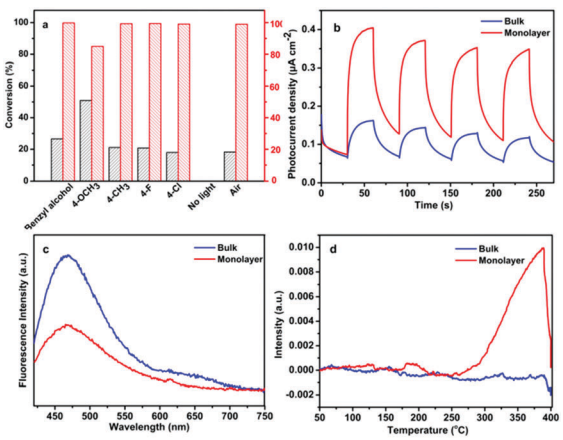

Fig. 2 (a) Conversion and selectivity for the photocatalytic oxidation of various benzyl alcohol derivatives over monolayer Bi_2MoO_6 nanosheets under light irradiation. Reaction conditions: catalyst: 16 mg, $\lambda \geq 400$ nm and 298 K. Reaction time: 4 h. (b) The photocurrent response of the Bi_2MoO_6 samples. (c) The room temperature photoluminescence spectra of the Bi_2MoO_6 samples at 397 nm. (d) The CO_2-TPD spectra of the Bi_2MoO_6 samples.

Published on 06 July 2017. Downloaded by Cornell University Library on 18/07/2017 13:28:58.

The BET surface areas of the monolayer Bi_2MoO_6 nanosheets and bulk Bi_2MoO_6 are about 16.4 and 7.4 $m^2\ g^{-1}$, respectively. The increased BET specific surface areas could adsorb more benzyl alcohol on the surface of the monolayer nanosheets with more active sites, thus contributing to improving the photocatalytic activity (Fig. S8, ESI†). Fig. 2b shows the photocurrents between the monolayer and the bulk. It can be clearly observed that the photocurrent of the monolayer is 4 times higher than that of the bulk. Such results incontrovertibly indicate that photoinduced electron–hole pairs are more easily separated on monolayer nanosheets than on the bulk, and so can participate in subsequent reactions. In addition, steady-state PL spectroscopy was performed to further understand this process (Fig. 2c). In particular, the intensity of the emission peak markedly reduced after the thickness of the orthorhombic Bi_2MoO_6 became that of a monolayer, which directly benefits effective charge separation.

More importantly, as is well-known, the surface basicity and acidity of the catalyst can play synergistic roles in selective photocatalytic organic transformation reactions. A high number of base sites for a photocatalyst is an extremely important factor for providing abundant adsorption sites for O_2, which leads to the easier activation of O_2.[25] Therefore, we performed temperature-programmed desorption experiments of CO_2 to investigate the Lewis basic sites over the Bi_2MoO_6 samples (Fig. 2d and Fig. S9, ESI†). The monolayers show a much higher intensity signal of TPD than the bulk, demonstrating that the Bi_2MoO_6 sample with a monolayer morphology could expose more Lewis basic sites that may originate from the Bi atoms on the surface of the nanosheets (Fig. S10, ESI†).[26,27] The Lewis acid sites on the Bi_2MoO_6 samples were investigated using *in situ* FTIR spectroscopy. As shown in Fig. 3a, two strong peaks at 1444 and 1575 cm^{-1} can be assigned to pyridine absorbed on the Lewis acid sites, which may derive from the Mo atoms on the surface of the monolayer nanosheets (Fig. S10, ESI†).[28] In comparison, these peaks on the bulk Bi_2MoO_6 are much weaker (Fig. 3b). It can also be seen that the monolayer nanosheets could expose many more acid sites than the bulk. In addition, the Lewis acid sites may act as the reactive sites.[29] Therefore, the strong basicity and Lewis acidity could facilitate the photocatalytic activity over the monolayer nanosheets. Furthermore, the *in situ* FTIR spectra of the Bi_2MoO_6 samples (Fig. 3c and d) reveal the chemisorption of abundant BA on the surface of the monolayer Bi_2MoO_6 nanosheets. As a result, the monolayer Bi_2MoO_6 nanosheets exhibit a much stronger capacity of adsorbing BA compared to the bulk. In addition, it is reported that producing more $O_2^{\bullet-}$ could contribute to the whole reaction.[30] As shown in Fig. S11 (ESI†), the increased signal intensities reveal that the monolayer Bi_2MoO_6 nanosheets could stimulate O_2 into $O_2^{\bullet-}$ species significantly better through electron transfer compared to the bulk. Furthermore, we also detected the formation of H_2O_2 in the reaction process (Fig. S12, ESI†).

On the basis of what has been discussed above, we propose a feasible reaction mechanism. From a thermodynamics point of view, UV-vis DRS spectroscopy (Fig. S13a and b, ESI†) reveals that the band gap energy of the monolayers is 2.45 eV, slightly bigger than that of bulk Bi_2MoO_6 (2.36 eV), which can be attributed to the quantum size effect. As indicated in Fig. S13c and d (ESI†), the Mott–Schottky measurements of the flat-band potential of bulk Bi_2MoO_6 and the monolayer Bi_2MoO_6 nanosheets were *ca.* −0.53 V and −0.54 V *vs.* Ag/AgCl at pH 6.8, respectively, which are equal to *ca.* −0.33 V and −0.34 V *vs.* NHE at pH 6.8, respectively. More importantly, the position of the conduction band (CB) over the two samples is more negative than the $O_2/O_2^{\bullet-}$ potential (−0.28 V *vs.* NHE).[31] According to the optical absorption spectrum, the valence band (VB) of the bulk and monolayer would occur at about 2.03 V and 2.11 V, respectively, and these values are more positive than the redox potential of benzyl alcohol oxidation (+1.98 V) (Fig. 4a).[32] From a kinetics perspective, BA and O_2 are absorbed on the Bi_2MoO_6 nanosheets in the dark. Under visible light illumination, the adsorbed oxygen is reduced by photogenerated electrons to superoxide radicals, and the photogenerated holes on the surface will induce benzyl alcohol to release protons directly under the auxiliary of $O_2^{\bullet-}$, which have difficulty in finishing the above steps on the bulk due to the recombination of the photogenerated carriers and the exposure of less active sites. In other words, the monolayers could provide not only more photoinduced electrons and holes but also many more active sites to accomplish the above consecutive steps. Moreover, superoxide radicals will further induce the complex to release protons in order to form benzaldehyde and H_2O_2. In the

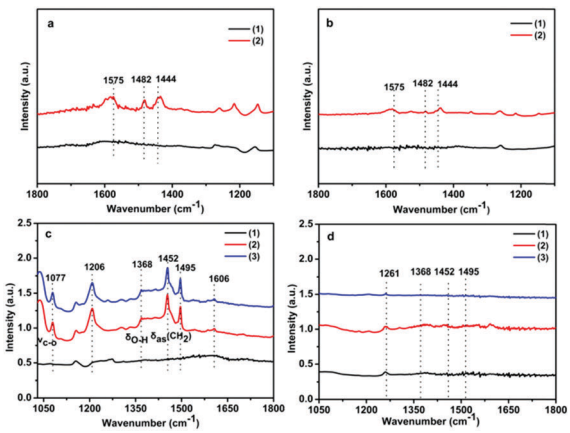

Fig. 3 *In situ* FTIR spectra of the monolayer Bi_2MoO_6 nanosheets (a and c) and bulk Bi_2MoO_6 disks (b and d) before and after the adsorption of pyridine (a and b) and benzyl alcohol (c and d). Conditions: (1) after degassing at 250 °C for 2.5 h. (2) Adsorption for 30 min at RT (physisorption + chemisorption). (3) Further evacuation of the excess probe molecules at 150 °C for 3 min under 6 × 10^{-4} Torr (chemisorption).

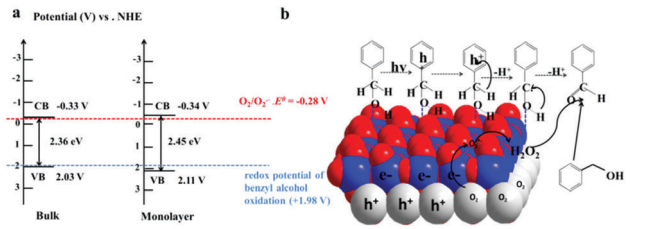

Fig. 4 (a) A schematic illustrating the electronic band structures. (b) A schematic illustration of the proposed feasible reaction mechanism for the selective oxidation of alcohols to the corresponding aldehydes over monolayer Bi_2MoO_6 nanosheets under visible light illumination. The atoms are color labeled: Bi (white), Mo (blue), and O (red).

Published on 06 July 2017. Downloaded by Cornell University Library on 18/07/2017 13:28:58.

meantime, the H_2O_2, as the formed intermediate, can react with the benzyl alcohol substrate. However, the existence of H_2O_2 turns out to have no obvious influence on the reaction process (Table S2, ESI,† entries 5–7). Afterwards, the formed H_2O_2 could also turn into H_2O *via* a series of reactions.

In summary, the monolayer Bi_2MoO_6 nanosheets are first synthesized *via* a surfactant-assisted route. The monolayer Bi_2MoO_6 nanosheets can remarkably boost the activity for the photocatalytic oxidation of benzylic alcohols, which is attributed to their molecular thickness, larger surface areas, ultrafast charge separation, higher capacity of oxygen activation, and the fact that they have more Lewis acid–base active sites and can form abundant surface complexes. We believe that this work will provide new insight into designing highly efficient and robust single layer nanosheet catalysts and transforming organic contaminants.

This work was supported by the National Natural Science Foundation of China (51672048 and 21677036) and the major science and technology projects of Fujian Province (2015YZ0001-1). S. Liang also thanks the Natural Science Foundation of Fujian Province for the Distinguished Young Scholars Fund (2016J06004).

Notes and references

1 G. Palmisano, V. Augugliaro, M. Pagliaro and L. Palmisano, *Chem. Commun.*, 2007, 3425–3437.
2 T. Ochiai and A. Fujishima, *J. Photochem. Photobiol., C*, 2012, **13**, 247–262.
3 Y. Qu and X. Duan, *Chem. Soc. Rev.*, 2013, **42**, 2568–2580.
4 S. N. Habisreutinger, L. Schmidt-Mende and J. K. Stolarczyk, *Angew. Chem., Int. Ed.*, 2013, **52**, 7372–7408.
5 S. I. Shin, A. Go, I. Y. Kim, J. M. Lee, Y. Lee and S.-J. Hwang, *Energy Environ. Sci.*, 2013, **6**, 608–617.
6 Y. Zhou, Y. Zhang, M. Lin, J. Long, Z. Zhang, H. Lin, J. C. Wu and X. Wang, *Nat. Commun.*, 2015, **6**, 8340.
7 Y. Liu, J. Xiong, S. Luo, R. Liang, N. Qin, S. Liang and L. Wu, *Chem. Commun.*, 2015, **51**, 15125–15128.
8 L. Liang, F. Lei, S. Gao, Y. Sun, X. Jiao, J. Wu, S. Qamar and Y. Xie, *Angew. Chem., Int. Ed.*, 2015, **54**, 13971–13974.
9 A. L. Linsebigler, G. Q. Lu and J. T. Yates, *Chem. Rev.*, 1995, **95**, 735–758.
10 T. Sivakumar Natarajan, H. C. Bajaj and R. J. Tayade, *CrystEngComm*, 2015, **17**, 1037–1049.
11 Y. Ma, Y. Jia, Z. Jiao, M. Yang, Y. Qi and Y. Bi, *Chem. Commun.*, 2015, **51**, 6655–6658.
12 J. Bi, L. Wu, J. Li, Z. Li, X. Wang and X. Fu, *Acta Mater.*, 2007, **55**, 4699–4705.
13 Y. Zhou, Z. Tian, Z. Zhao, Q. Liu, J. Kou, X. Chen, J. Gao, S. Yan and Z. Zou, *ACS Appl. Mater. Interfaces*, 2011, **3**, 3594–3601.
14 M. Long, W. Cai and H. Kisch, *Chem. Phys. Lett.*, 2008, **461**, 102–105.
15 B. Zhang, J. Li, Y. Gao, R. Chong, Z. Wang, L. Guo, X. Zhang and C. Li, *J. Catal.*, 2017, **345**, 96–103.
16 M. Anpo and J. M. Thomas, *Chem. Commun.*, 2006, 3273–3278.
17 S. Liang, L. Wen, S. Lin, J. Bi, P. Feng, X. Fu and L. Wu, *Angew. Chem., Int. Ed.*, 2014, **53**, 2951–2955.
18 J. Li, Y. Yu and L. Zhang, *Nanoscale*, 2014, **6**, 8473–8488.
19 Y. N. Zhu, J. J. Mu, G. H. Zheng, Z. X. Dai, L. Y. Zhang, Y. Q. Ma and D. W. Zhang, *Ceram. Int.*, 2016, **42**, 17347–17356.
20 H. Li, Q. Deng, J. Liu, W. Hou, N. Du, R. Zhang and X. Tao, *Catal. Sci. Technol.*, 2014, **4**, 1028.
21 Y. S. Xu and W. D. Zhang, *Dalton Trans.*, 2013, **42**, 1094–1101.
22 Z. Zhao, W. Zhang, Y. Sun, J. Yu, Y. Zhang, H. Wang, F. Dong and Z. Wu, *J. Phys. Chem. C*, 2016, **120**, 11889–11898.
23 H. Huang, K. Liu, K. Chen, Y. Zhang, Y. Zhang and S. Wang, *J. Phys. Chem. C*, 2014, **118**, 14379–14387.
24 J. Xiong, L. Wen, F. Jiang, Y. Liu, S. Liang and L. Wu, *J. Mater. Chem. A*, 2015, **3**, 20627–20632.
25 H. Metiu, S. Chrétien, Z. Hu, B. Li and X. Sun, *J. Phys. Chem. C*, 2012, **116**, 10439–10450.
26 D. Guo, R. Shibuya, C. Akiba, S. Saji, T. Kondo and J. Nakamura, *Science*, 2016, **351**, 361–365.
27 H. Li, F. Qin, Z. Yang, X. Cui, J. Wang and L. Zhang, *J. Am. Chem. Soc.*, 2017, **139**, 3513–3521.
28 Y. Liu, T. Gu, Y. Wang, X. Weng and Z. Wu, *Catal. Commun.*, 2012, **18**, 106–109.
29 T. Shishido, K. Teramura and T. Tanaka, *Catal. Sci. Technol.*, 2011, **1**, 541.
30 N. Zhang, X. Li, H. Ye, S. Chen, H. Ju, D. Liu, Y. Lin, W. Ye, C. Wang, Q. Xu, J. Zhu, L. Song, J. Jiang and Y. Xiong, *J. Am. Chem. Soc.*, 2016, **138**, 8928–8935.
31 S. Naya, T. Niwa, R. Negishi, H. Kobayashi and H. Tada, *Angew. Chem., Int. Ed.*, 2014, **53**, 13894–13897.
32 X. Xiao, J. Jiang and L. Zhang, *Appl. Catal., B*, 2013, **142–143**, 487–493.

 This journal is © The Royal Society of Chemistry 2017